Chapter 6: Fixed Bed Reactor Modelling

6.1 Introduction

In this chapter an advanced reactor model is developed and solved using a numerical software code to predict the experimental data obtained from a catalytic packed bed reactor system. A description is provided about the experimental apparatus used to generate experimental results. A CAD geometry was generated for a randomly packed bed consisting of cylindrical pellets with a variation in pellet size distribution. An axi-symmetrical cross sectional slice is taken through the 3D model to be a representative heterogeneous geometry of the bed. The governing equations, numerical solution and mesh procedure are discussed. The advanced heterogeneous reactor model is solved and compared with experimental results. Average conversion and centreline temperature profiles are used to validate the accuracy of model.

6.2 Description of Reactor Structure

The sulphur trioxide decomposer was thoroughly discussed in Chapter 5 and in this section a short description is given, with emphasis on the 100 mm bed section which was utilized to obtain experimental results in the residence time variation section (Section 5.3.2.3). In Figure 6-1 a schematic is shown of the reactor tube in furnace with thermocouple placements of the centreline as well as the wall. Although the spacing is not precise on the drawing the distances are indicated. The two different regions can also be observed, i.e. the pre-heating section and catalyst section. For modelling purposes the 100 mm catalyst section was modelled with no attention given to the pre-heating section, except to obtain initial conditions to the catalytic bed. Certain assumptions were made for the inlet conditions to the catalyst section and will be given in following sections. Pure sulphuric acid was decomposed into sulphur trioxide in the vaporizer and sulphur trioxide was decomposed in the reactor over the 100 mm bed section filled with catalyst pellets. To determine the amount of conversion achieved a mass balance

was conducted over the experimental apparatus in which the amount of sulphur dioxide formed, oxygen formed, sulphuric acid condensed (mass and concentration), as well as sulphur dioxide in scrubbers, were measured. The experimental results obtained in Section 5.2.2.3 (Variation in residence time) were used for modelling purposes (average outlet conversion, centreline and wall temperature). For further details about the operating procedure, as well as experimental apparatus and results, see Chapter 5.

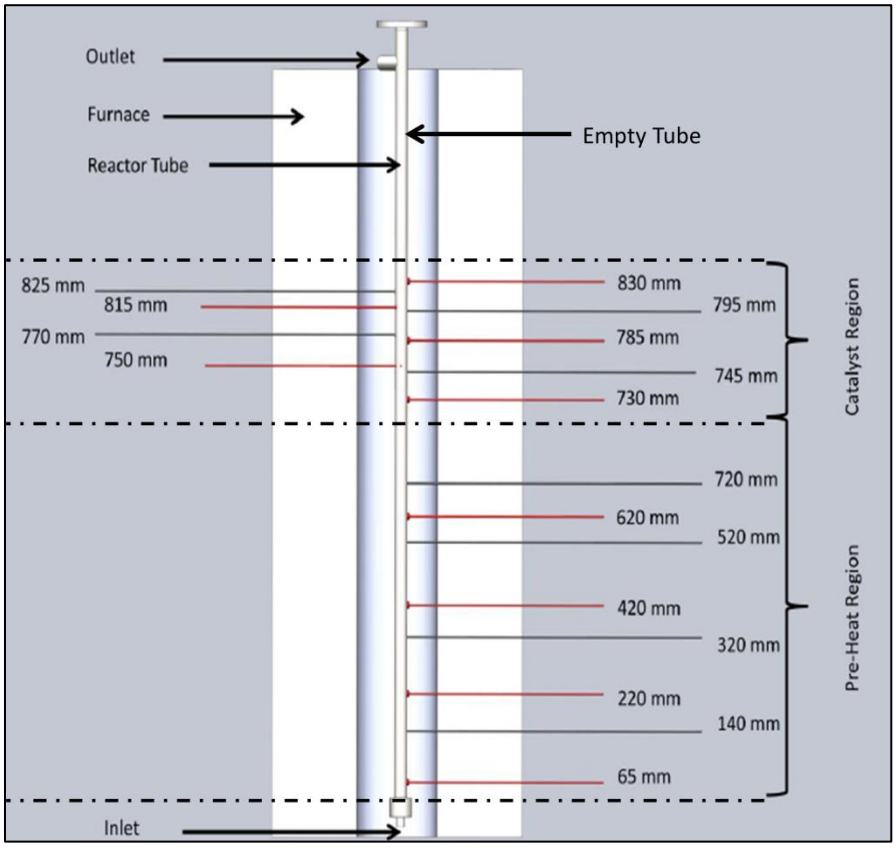

Figure 6-1: Reactor (100 mm bed section) with thermocouple placements

6.3 Structure of Packing

The geometry of a Computational Fluid Dynamic (CFD) model can be one of the limiting factors, especially in chemical reactor engineering where the random packing of a reactor bed usually consists of cylindrical pellets with a pellet size distribution in radial and axial dimensions. The other challenge is getting a realistic drawing that will give an accurate representation of the real packing with regard to void fraction and pellets orientation in the geometry. Various methods have been identified as mentioned in Chapter 2 and the geometry for this project was generated with the software code

DigiPac™ which has been verified in literature to give accurate void fractions for a specific spacing geometry under investigation (Caulkin, 2009) (Caulkin, 2006). Geometry was created by DigiPac™ with the following specifications: length of tube was 100 mm with number of particles 2 786. The number of pellets used in the model geometry as described was 2 786 for the 100 mm bed section while the approximate number of pellets used in an experiment for average pellet conditions delivered 2568 pellets-an error of 8%. The file size in STEP form was 250 mb which is quite large for COMSOL MultiPhysics® 4.3b to import and define the specific physics without having problems with the hardware. The reason for the large file is that the particles and structures are composed of polygons to form a shape. The more polygons the better accuracy is obtained of the structure authenticity but in turn larger file size. The file size was reduced in order to reduce the amount of polygons without influencing the integrity of the structure. Figure 6-2 gives a representation of a part of the geometry with the polygons that constructed the catalyst pellets.

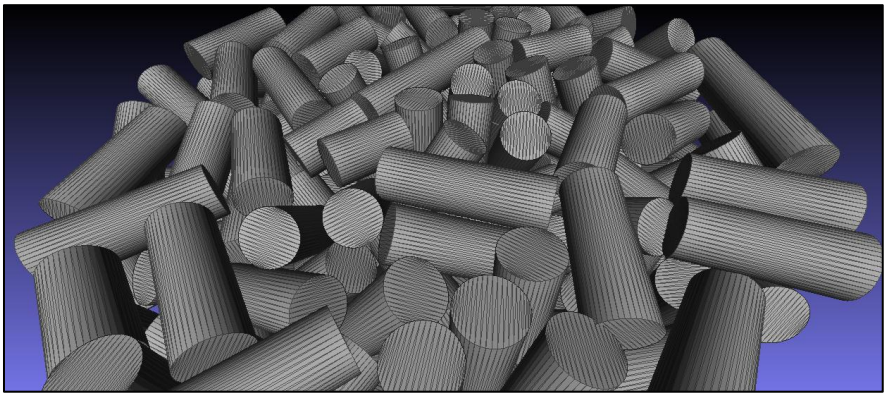

Figure 6-2: Geometry of packed bed of pellets created from polygons

Valuable data that can be obtained from the DigiPac™ geometry is density distribution in the radial and axial direction at any coordinates. The pellet size distribution supplied was evaluated experimentally by choosing a sample of 100 random pellets and measuring the diameters and lengths of the cylindrical pellets. Figure 6-3 shows the pellet size distribution in mm and numbers indicated on each bar represent the percentage in that specific range.

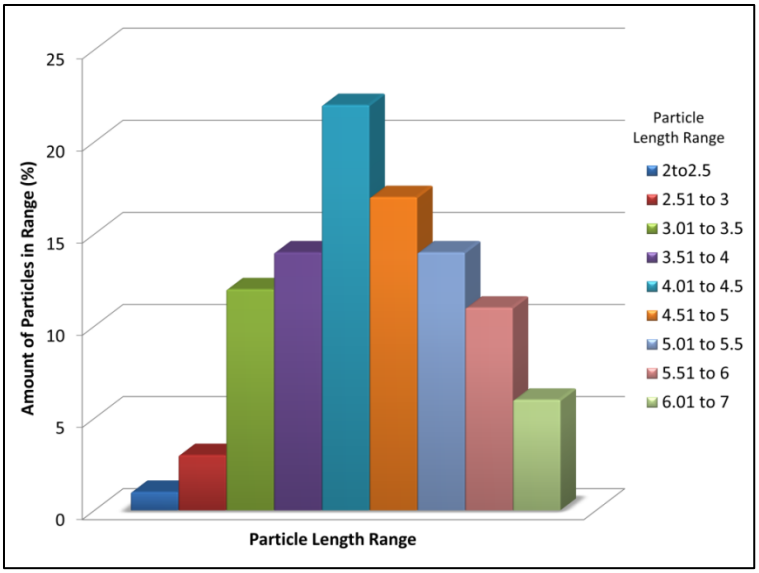

Figure 6-3: Pellet size distribution of cylindrical catalyst pellets as evaluated experimentally (length in mm)

Figure 6-4 above gives an illustration of the 3D geometry with the packing and pellet size distribution as determined experimentally.

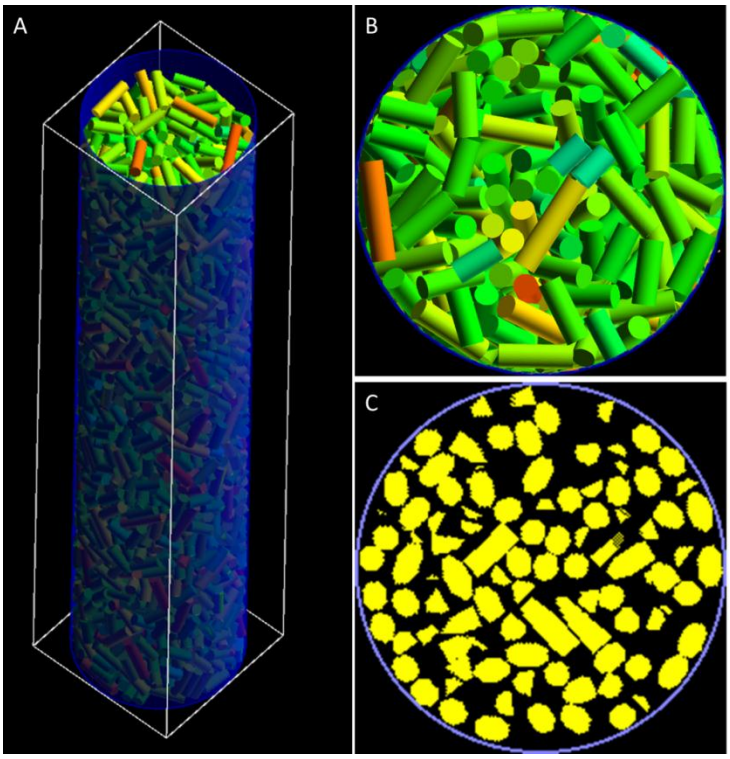

Figure 6-4: Geometry by DigiPac™; A: 3D rendering of cylinder filled with pellets; B: Geometry rendering at top of cylinder; C: Cross section of packing in a plane

A top view of the rendered geometry can be seen in Figure 6-4: B with a cross sectional view at a point in the axial direction to get an idea of the integrity of the geometry in C. A two dimensional cross section was taken through the cylinder of packed pellets at various intervals in one radial direction across the tube diameter in Figure 6-5.

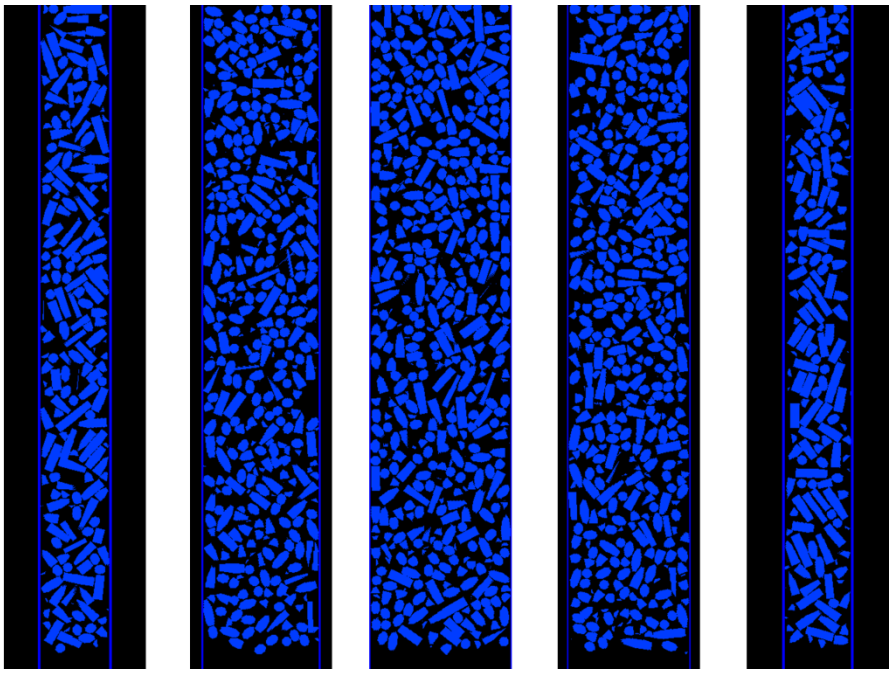

Figure 6-5: Cross sectional illustrations of packed bed geometry at various sections in the radial direction

Due to the expensive computational resources required to solve geometry as complex as the randomly packed bed, a 2D cross sectional image was generated, as in Figure 6-5: A, and transforming it into CAD geometry to be imported into COMSOL MultiPhysics® 4.3b and solved as a 2D axi-symmetrical model. The 2D model requires significant computational time to solve the model and still provided an accurate representation of the solid-fluid interaction in the model. The CAD file representing a 2D cross section of the packing was imported, physics defined and solved. The void fraction of the packing is vital in CFD simulations to obtain accurate results specifically with regard to pressure drop over the packing.

The software code DigiPac™ generated profiles for the void fraction distribution along any coordinates desired. Figure 6-6 illustrates the distributions of the void fraction in the axial direction. These figures are consistent with literature (van Antwerpen, 2009) of the void fraction distribution, especially in the direction where the densest part of the packing is in the centre and the void fraction increases

exponentially towards the tube wall. The packing generated has a larger void fraction than evaluated experimentally. This could be due to the non-homogeneity of the TiO_2 pellets which change phase from anatase to rutile, thus causing a morphological change in the cylindrical pellet. The error could be from the pellet size distribution supplied to generate the specific bed. However, with the large distribution in pellet sizes it is improbable to get an accurate representation of the distribution and thus the bed void packing is assumed to be an accurate representation of the geometry.

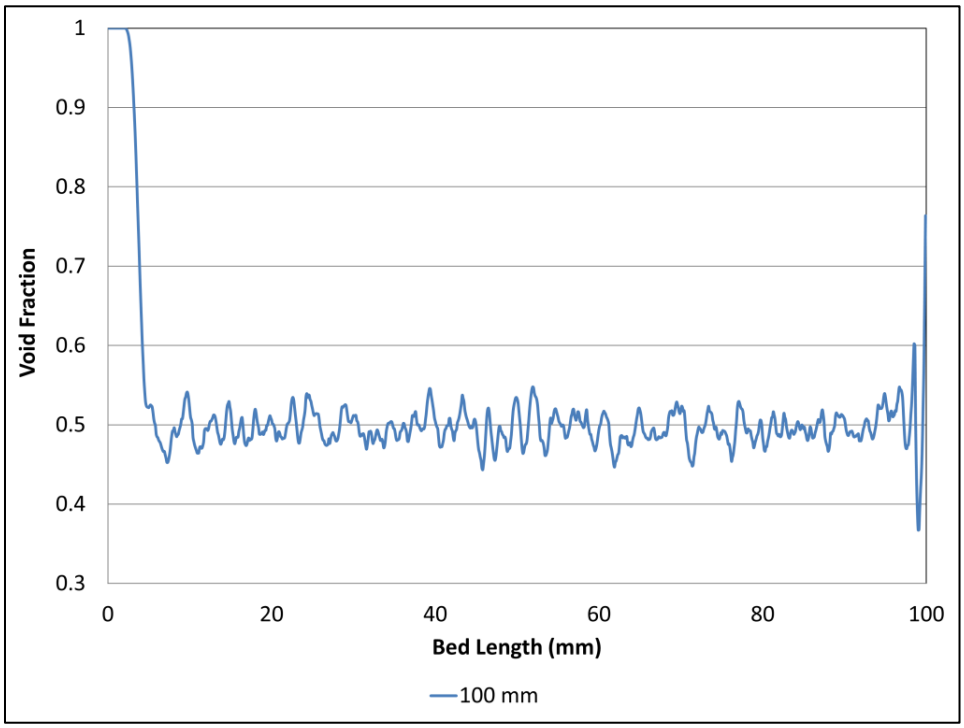

Figure 6-6: Void fraction distribution along axial (z) direction for 100 and 400 mm beds

The radial void fraction was evaluated by DigiPac™ and can be seen from Figure 6-7. The 2D heterogeneous model was developed with the geometry as discussed in COMSOL Multiphysics® 4.3b.

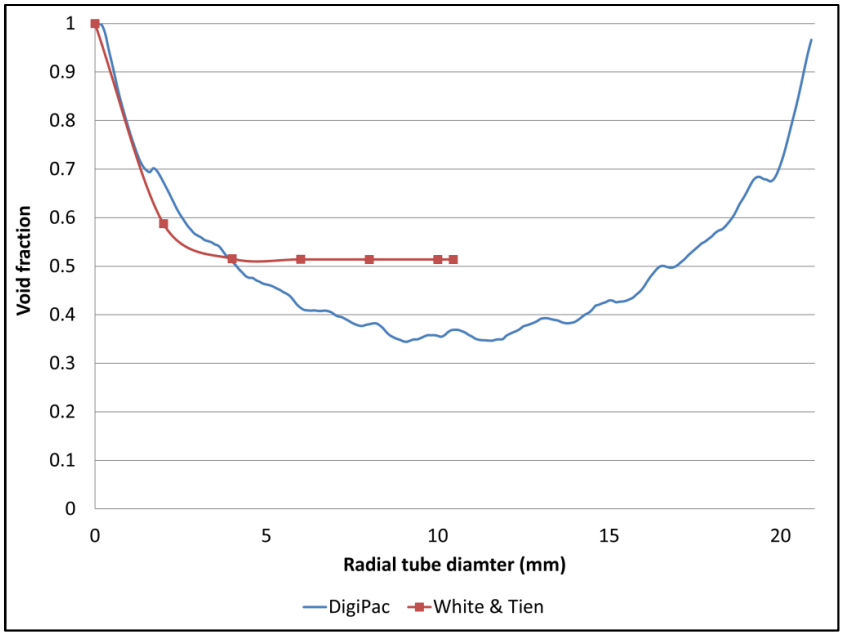

Figure 6-7: Void fraction distribution in radial (X) tube direction

An empirical porosity correlation from White & Tien (van Antwerpen, 2009) was used to predict the porosity and compare against the results obtained by DigiPac™ for porosity variation in the radial direction. The porosity predicted by White & Tien is a exponential function and as a result does not indicate the oscillating void spaces. The correlation gives a decent indication of the porosity distribution as was predicted by the software code, when taken into consideration that a constant particle diameter was used with the empirical correlation, while DigiPac™ predicts with a particle size range. One the main restrictions for CFD coupled with reaction simulations, as mentioned, are the geometry used to represent the reactor system under investigation. The CAD file in itself is very complicated and loaded with data, thus requiring the geometry to be simplified in order to be solved.

6.4 Reactor Modelling

6.4.1 Governing Equations

The reactor system was modelled and to account for the effects of momentum, heat and mass standard governing equations were applied. The 2D axi-symmetrical cross sectional model was used as it gave a representation of the system with packing along the length of the catalyst bed with a true representation of the random packing. An axi-symmetrical model had to be used to ensure that the

correct transport mechanisms were incorporated in the model. To solve the geometry with the applicable governing equations together with boundary conditions, certain assumptions were made:

- Two phases consisting of a fluid phase and a catalyst phase with interactive heat and mass transfer with an endothermic chemical reaction in the catalyst phase.
- Heat was transferred from the wall to the flowing gas (and catalyst) by convection and conduction with radiation applied.
- Radiation was accounted for by means of a empirical correlation from literature with an adjusted effective thermal conductivity in the fluid phase.
- A 2D axi-symmetrical geometry was assumed to be a representative model for packed bed in tube.
- The inlet flow to the model was assumed as plug flow and the entry region was small so that the flow distribution would take on the flow patterns of the geometry short after entry.

The 100 mm length cross section will be used to show where the physics and boundary conditions were defined in Figure 6-8.

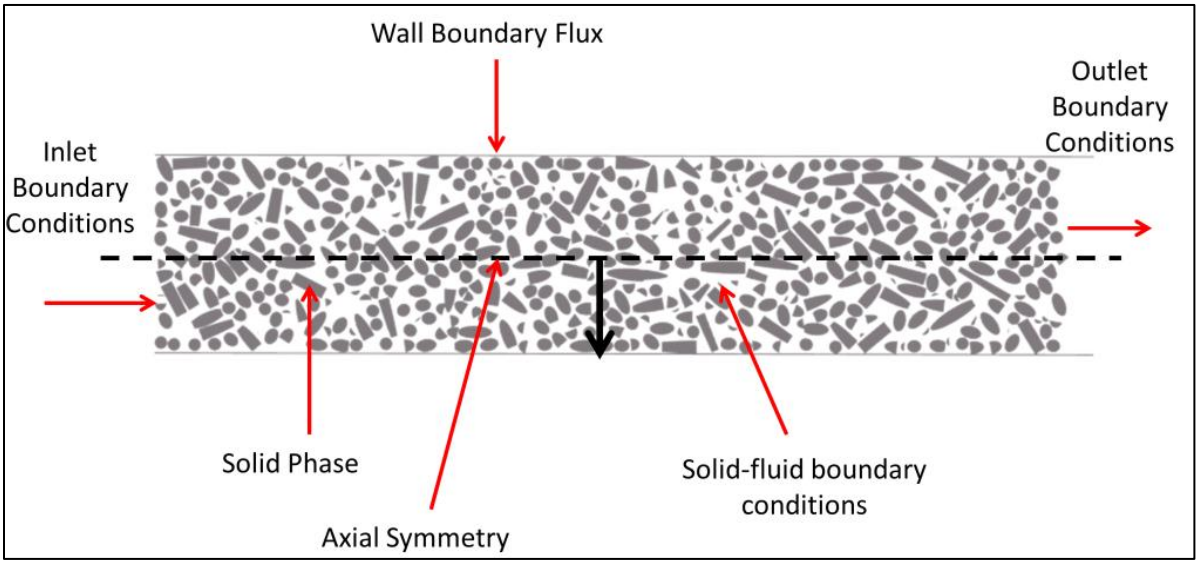

Figure 6-8: Representative 2D cross sectional geometry of packed bed with boundary conditions

The equations used to describe continuity, momentum, heat and concentration are given as follows (Nield, 2006) (COMSOL, 2013):

Continuity:

$$\nabla.\left(\rho u\right)=0 \qquad [59]$$

Momentum:

$$\rho_f\left(\left(u\cdot\nabla\right)u\right)=\nabla\cdot\left[-PI+\mu_f\left(\nabla u+\left(\nabla u\right)^{\mathrm{T}}\right)-\frac{2}{3}\mu_f\left(\nabla\cdot u\right)I\right] \qquad [60]$$

Heat:

$$\nabla.\left(-\lambda\nabla T\right)+\rho c_p u.\nabla T=Q \qquad [61]$$

Concentration:

$$\nabla.\left(-D_i\nabla C_i\right)+u\nabla C_i=r_A \qquad [62]$$

Boundary Conditions:

$T_w=T_{Exp}$	at wall
$\nabla C_A=0$	at wall
$u=0$	at wall and on all particles
$C_A=C_{A0}$	at inlet
$T_f=T_{f0}$	at inlet
$p=p_0$	at outlet
$u=u_0$	at inlet

The conservation equations supplied for continuity, momentum, heat and mass are standard equations with the applicability to the solid and fluid phase, respectively, are summarized in Table 6-1:

Table 6-1: Applicability of parameters to conservation equations

		Catalyst Phase	Fluid Phase	Units
Thermal Conductivity	λ_i	Titania	Gas fluid phase	$W/m.K$
Heat Sources	Q	Reaction Heat and Reaction Rate; Radiation	-	W/m^3
Diffusion	D_i	Molecular and Knudsen	Molecular	m^2/s
Reaction	R	Reversible Reaction Rate	-	$mol/m^3.s$

The parameters given in Table 6-1 provide the distinction made between the fluid and solid phase. In the solid phase effective diffusivity and thermal conductivity of the catalyst support (titania) are supplied together with a reaction rate and heat of reaction. In the fluid phase thermal conductivity of process gas and molecular diffusion are parameters specified. The Navier Stokes equation (60) is used to supply the convective transport phenomena and since a no-slip boundary condition is applied the parameters mentioned above and specified will be the driving force at the interface between solid and fluid phase. The main idea of the heterogeneous model is to specify transport parameters and see how the packing of the pellets in a random orientation will influence the fluid flow around the pellets and in turn influence the transport between phases. Weakly compressible flow is assumed to be present. The particle and tube Reynolds number was determined as 16 and 200 respectively. This is again in the low laminar flow regime and although the particle Reynolds number is in the transition region (Baker, 2012), the aspect ratio of tube diameter to pellet diameter is above 10, which indicates that well dispersed flow is present in the packing, nullifying recirculation effects.

The equations used in this model are the same as were used in the overall kinetic model (Chapter 4) with the exception that radiation was included into this model. Due to the complexity and uncertainty of implementing radiation in a packed bed of pellets the empirical correlation from Bauer & Schlünder (1978) in Appendix A was used to adjust the thermal conductivity in the convective stream to account for radiation. A combination of convective and radiation heat transfer was included since conduction

was accounted for in the catalyst pellets. The effective emissivity was taken as 0.05 for the platinum in the catalyst pellets (Incropera & DeWitt, 2002). The wall temperature was supplied as a polynomial function that was fitted using the experimental results obtained for measurements on the tube wall.

Dispersion of mass in the fluid phase was only accounted for with molecular diffusion. Molecular diffusion, effective diffusion (porosity and tortuosity) and Knudsen diffusion were equated in the same manner as described in Chapter 4 and was applicable to the catalyst pellets. The values of the parameters, as well as thermal properties used in this model, are given in Appendix G. The reversible reaction rate equation from Chapter 4 was used as the rate equation with the activation energy and pre-exponential factor of 165.9 kJ/mol and 1.24×10^{12} s^{-1} respectively where the equation is given as:

$$r_A = -k_{fr}\left(C_{SO_3} - \frac{C_{SO_2}C_{O_2}^{0.5}}{K_{eq}}\right) \quad [63]$$

The quantities investigated in the model which was of concern was as follows:

- Average conversion achieved
- Concentration distribution in fluid and solid
- Temperature distribution in fluid and solid
- Centreline temperature profiles to compare against experimental data

6.4.2 Numerical Solution and Procedure

The geometry as generated in Section 6.3 was imported into the numerical software code COMSOL MultiPhysics® 4.3b where it was discretised and the applicable equations applied to specific domains. The mesh was constructed by assigning boundary layers on the side of the larger tube (fluid phase) as well as on the interface of the catalyst particles (fluid/solid phase), with the number of layers varying. The volume of the geometry was constructed by Free Tetrahedral elements which were set to grow from fine to coarse, fine at the wall and interfaces to coarse in the general domain.

The solver chosen for the system was a DIRECT PARDISO solver with an error tolerance of $1e^{-3}$ (COMSOL, 2013). The discretization method was chosen as linear which was found to be sufficient in terms of

stabilization in the model. The computations were completed on a GNOME computer, Linux operating system with 18 processors and 252 GB RAM.

6.5 Results and Discussion

6.5.1 Geometry Mesh

The mesh generated on the geometry consisted of a variety of boundary layers, as well as Free Tetrahedral elements. The mesh generated can be seen in Figure 6-9 where a partial section of the geometry with mesh generated is indicated.

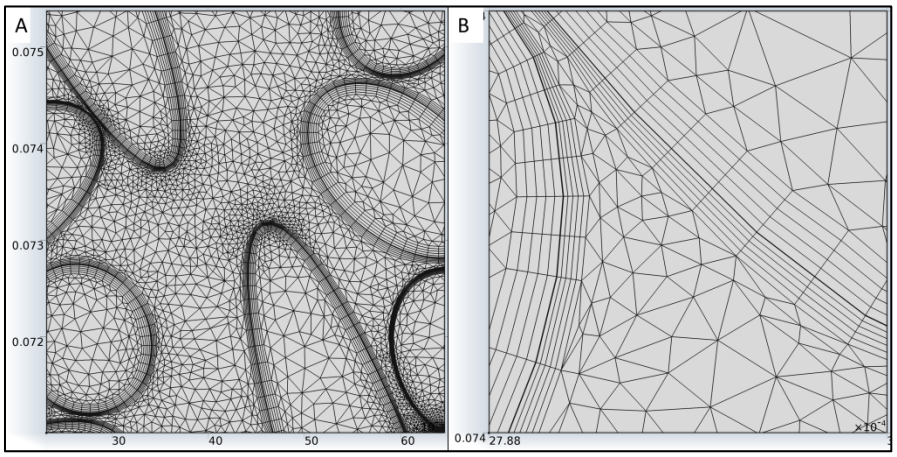

Figure 6-9: Final mesh (partial) generated on the geometry

The mesh generated on the geometry consisted of approximately 732 000 elements (combined boundary layers as well as Free Tetrahedral). All elements were inserted with a growing factor from fine to coarse but due to the complexity of the geometry complete mesh refinement could not be done on all boundaries since various boundaries were touching or very close to each other.

6.5.2 Packed Bed Model Results

The results obtained from the cross slice model are discussed in this section where results include velocity distribution, centreline temperature profiles, average outlet conversion as well as concentration distribution. Due to the number of results generated in the models for all the experimental work completed, the results of only one model will be shown and discussed in detail and the combined conversion and temperature profiles will be discussed and compared.

(I) Velocity

The velocity distribution in a randomly packed bed with irregular cylindrical shapes is important since the dominant driving force for species out of the system is convection. The velocity distribution given in Figure 6-10 is along the length of the reactor length.

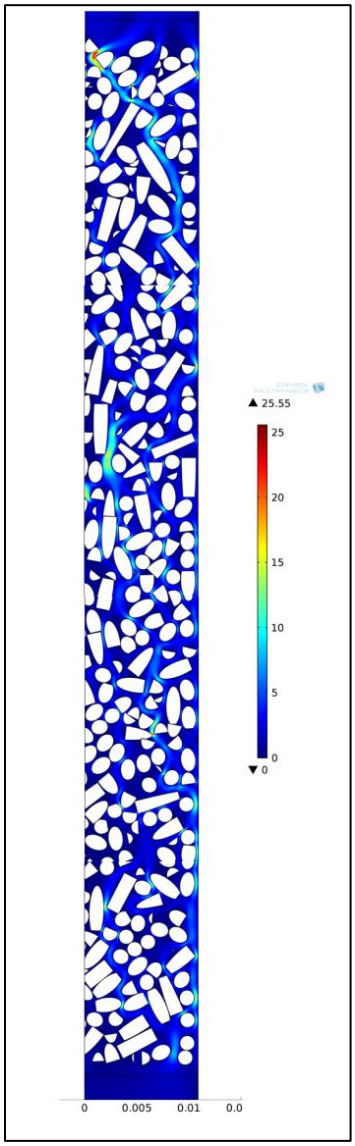

Figure 6-10: Velocity distribution along the length of catalyst bed (m/s)

The colour in the images provides visual aid to illustrate the more dominant convective streams as a result of the packing and a path of least obstruction. The velocity distribution illustrates the no-slip boundary condition, as well as areas where velocity is very low and molecular diffusion is the driving force to transport species.

(II) Heat Distribution

The temperature distribution in the model is quite important as it could provide information on cold spots in the reactor as well as radial profiles as a result of the high endothermic nature of the reaction. The temperature distribution in the fluid and solid phases can be seen Figure 6-11 and the figure indicates that just after the inlet a rather large cold spot exists.

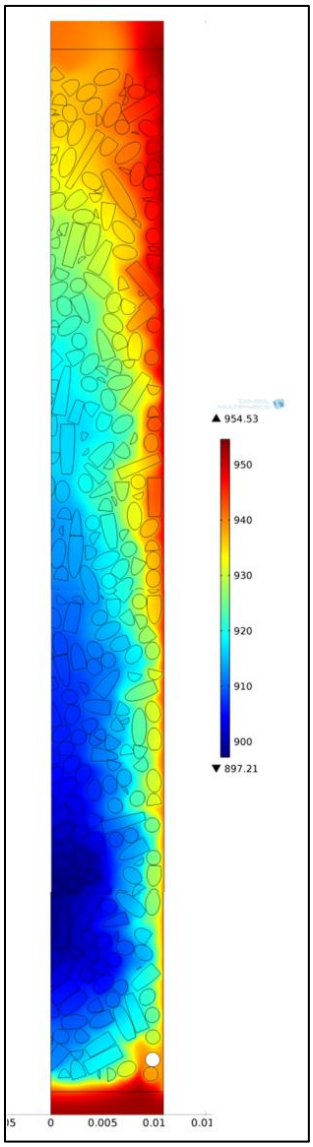

Figure 6-11: Temperature distribution in both fluid and catalyst phase (K)

This is due to the reaction rate, which has an exponential nature, which is fast initially whereas the concentration and temperature are also high, resulting in high conversion. As the heat is consumed and concentration converted the reaction rate slows down and the rate of heat transfer is sufficient to

supply heat for reaction as well as increase the temperature of the process gas. A radial profile for temperature at length of 0.05 m as well as the fluid/solid interface for heat distribution can be seen in Figure 6-12.

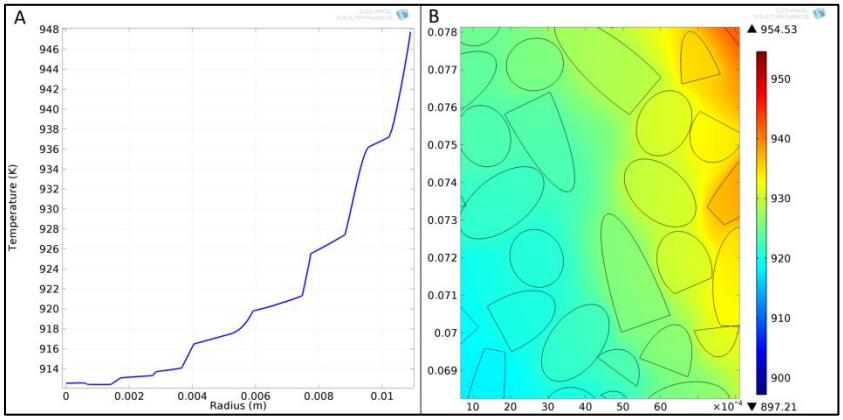

Figure 6-12: Temperature distribution in model (K); A: Radial temperature distribution at x = 0.05 m; B: Temperature distribution between pellet and fluid (K)

From Figure 6-12 it can be seen that at the specific coordinates quite a large temperature variation occurs in the radial direction which is also indicated in Figure 6-11 where a dark blue colour indicates cold temperatures. This is all attributed to the endothermic nature of reaction consuming heat as sulphur trioxide is consumed. When looking at Figure 6-12 (B) it seems that at the specific section that there is not a big difference between the temperature in the fluid and catalyst pellets. The centreline temperature profile was measured experimentally and it was compared against the model prediction generated.

Due to physical restrictions thermocouples could not be placed nearer to the inlet of the bed. The centreline temperature probes measurements experimentally were compared at each point to the model prediction rather than visualizing on a plot. The 1st probe measurement was not compared since that was the inlet specified boundary condition. The second probe as seen in Figure 6-1 in the catalytic bed region was discarded due to inaccurate operation. The last three measurements in the 100 mm bed section were measured and used to compare the data in terms of percentage error in Table 6-2 where the experimental temperature (T_{ex}) the model temperature (T_m) as well as error percentage (Err) are given.

Table 6-2: Centreline temperature absolute error (%) between model and experimental value

Velocity: 1 m/s													
Tc Placement		**903 K**			**953 K**			**1003 K**			**1053 K**		
	mm	**T_{ex} (K)**	**T_m (K)**	**Err (%)**	**T_{ex} (K)**	**T_m (K)**	**Err (%)**	**T_{ex} (K)**	**T_m (K)**	**Err (%)**	**T_{ex} (K)**	**T_m (K)**	**Err (%)**
1	55	891	885	0.7	921	915	0.7	981	970	1.1	1035	1020	1.5
2	85	894	890	0.4	930	930	0.8	994	984	1.0	1053	1036	1.6
3	100	891	895	0.5	940	940	1.2	991	990	0.1	1051	1045	0.6
Velocity: 1.2 m/s													
1	55	897	886	1.2	929	914	1.6	971	960	1.1	1024	1010	1.4
2	85	896	887	1.0	939	924	1.6	983	975	0.8	1042	1030	1.2
3	100	892	892	0.0	936	930	0.6	981	986	0.5	1041	1040	0.1
Velocity: 1.32 m/s													
1	55	900	886	1.6	932	913	2.1	978	960	1.8	1023	1015	0.8
2	85	903	887	1.8	939	923	1.7	983	976	0.7	1035	1033	0.2
3	100	901	892	1.0	936	935	0.1	979	985	0.6	1033	1042	0.8

The inlet probe was at length 730 mm (taken as base = 0) in Figure 6-1 with other probes placements indicated in Table 6-2. Thus the centreline temperature profile was compared against results from thermocouple points. The highest error was found to be 2 % and the lowest is 0 % thus indicating that the temperature prediction by the model was quite accurate. Again it has to be mentioned that the thermocouples probe placement in the radial direction was assumed to be in the centre as there was no easy inexpensive way to verify the coordinates. Thus the placement of the thermocouple probes could be slightly off and with a error of 2% can then be taken as accurate predictions.

(III) Concentration Distribution

The concentration distribution inside of the packing is quite important since better distribution and exposure to catalyst surface the more conversion can be achieved. The concentration distribution of sulphur trioxide in both the fluid and catalyst phase can be seen in Figure 6-13.

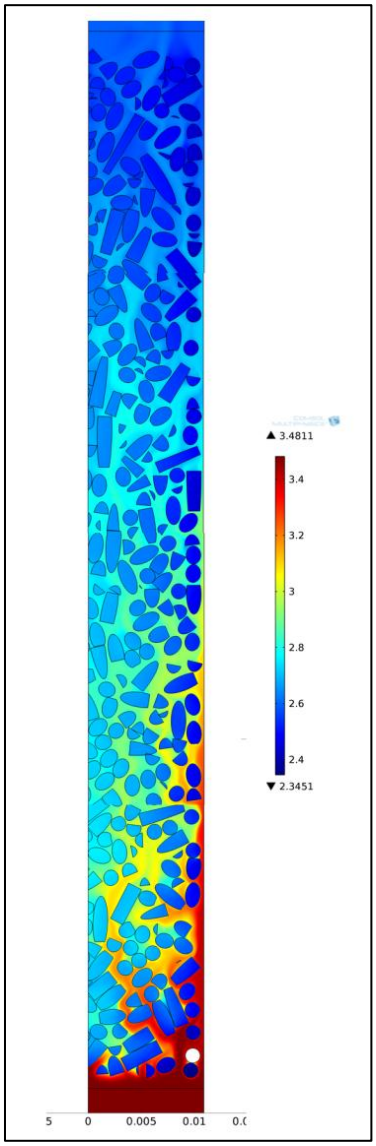

Figure 6-13: Concentration distribution of sulphur trioxide in both fluid and catalyst phase (mol/m^3)

Although difficult to see a trend through all of the particles it is noticeable that the inlet concentration in the fluid phase is high and as it progresses through the model the concentration available for conversion decrease due to reaction. The amount of conversion is high initially due to the high temperature and exponential nature of the reaction rate at the inlet. As sulphur dioxide and oxygen are produced and

the temperature changes the local equilibrium changes and thus the amount of sulphur trioxide that can be converted also changes. The centreline distribution of sulphur trioxide, sulphur dioxide and oxygen can be seen along the length of the reactor tube in Figure 6-14. The profiles for the three species show the correct trend for every mole of sulphur trioxide converted, sulphur dioxide is produced and a half mole oxygen.

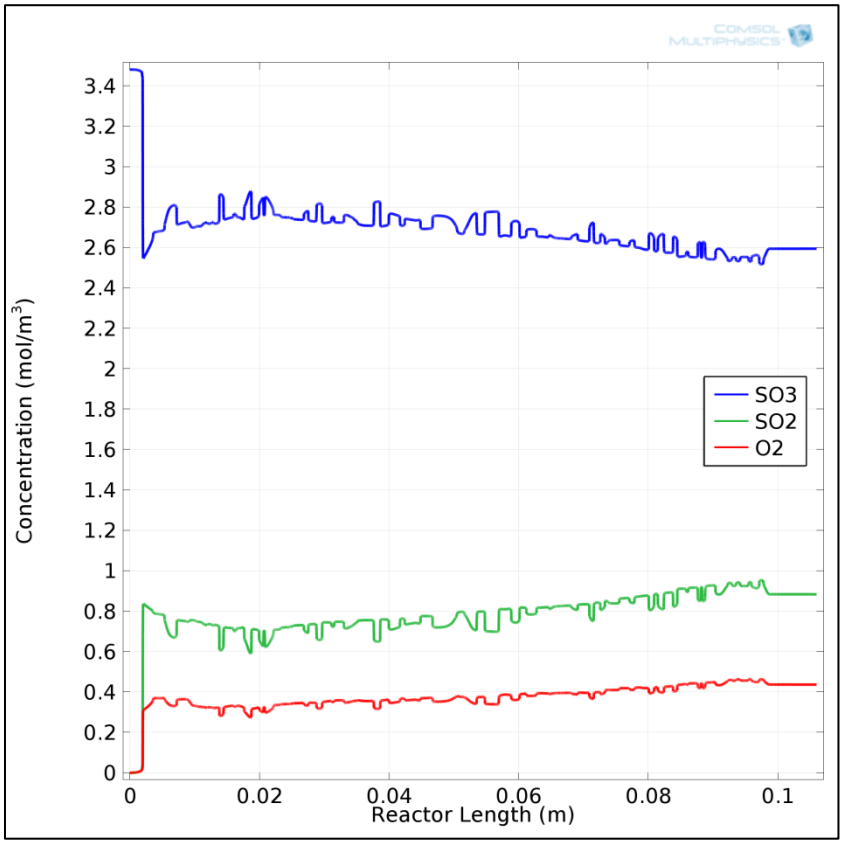

Figure 6-14: Centreline concentration distribution

The centreline concentration profile as observed in Figure 6-14 indicates, although on a shorter catalyst packing, that the WHSV trend in Figure 5-19 could be explained by the model as most conversion is achieved as the process gas enters the bed, after which the conversion changes with a change in temperature (equilibrium). A definite trend with regard to concentration radial profiles can be observed from Figure 6-13 and this is also seen from Figure 6-15 where a radial profile (at length 0.05m) indicates the small but present profiles. Again the stoichiometric relation is observed, for every mole of sulphur trioxide converted one mole sulphur dioxide forms as well as half a mole oxygen. The radial concentration distribution, as well as concentration distribution between fluid and solid phase, can be seen in Figure 6-15.

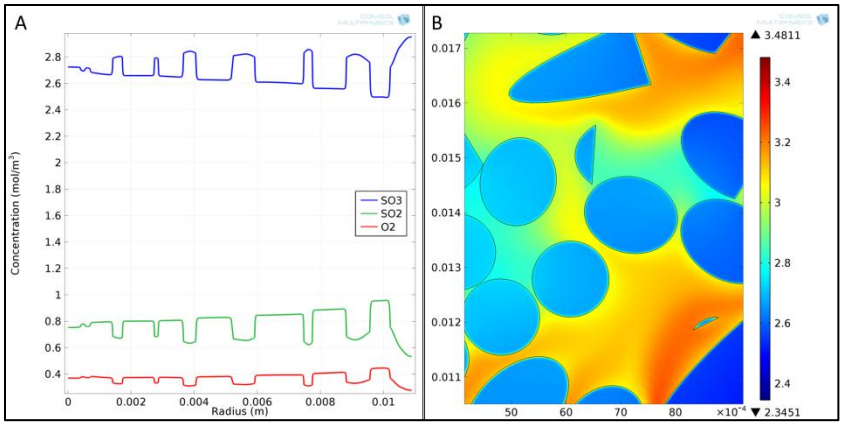

Figure 6-15: Concentration distribution (mol/m^3); A: Radial concentration variation at x = 0.05 m; B: Concentration distribution between pellet and fluid

Similar trends can be observed as in Chapter 4 where the concentration in the fluid is quite higher and the conversion achieved takes place in boundary layers of the catalyst particles where equilibrium ultimately stops the forward reaction as products start to form. Except on the boundary the concentration distribution inside the particles is quite homogeneous. The average conversion achieved over the catalytic bed was measured and is one of two parameters to be used to evaluate the accuracy of the model. The average conversion achieved experimentally, equilibrium conversion and the average conversion determined by the model for the various process conditions can be seen in Figure 6-16, Figure 6-17 and Figure 6-18.

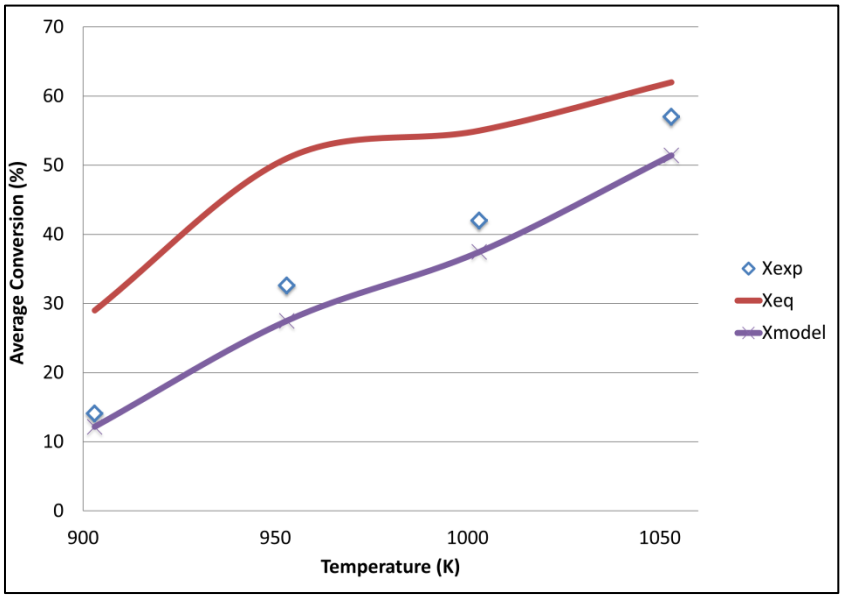

Figure 6-16: Average conversion by model versus experimental for flow: 1 m/s

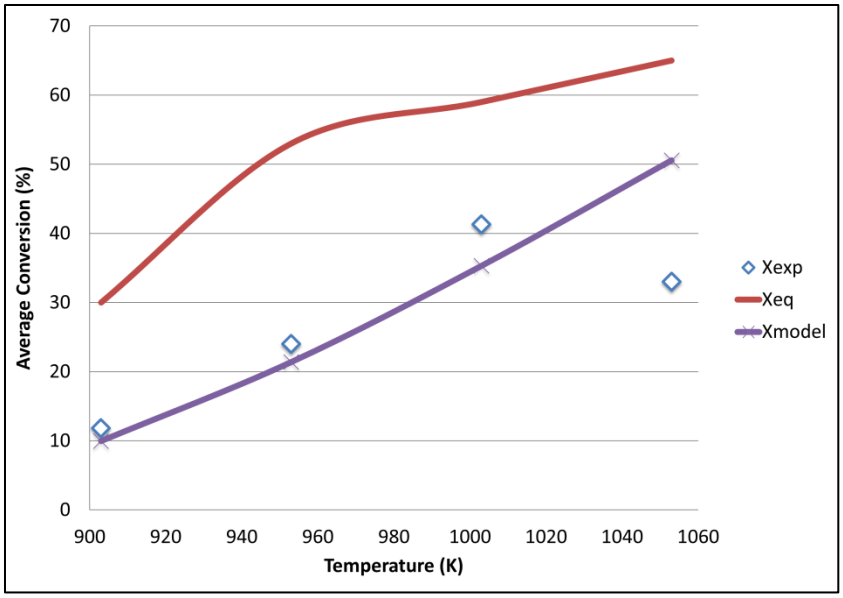

Figure 6-17: Average conversion by model versus experimental for flow: 1.23 m/s

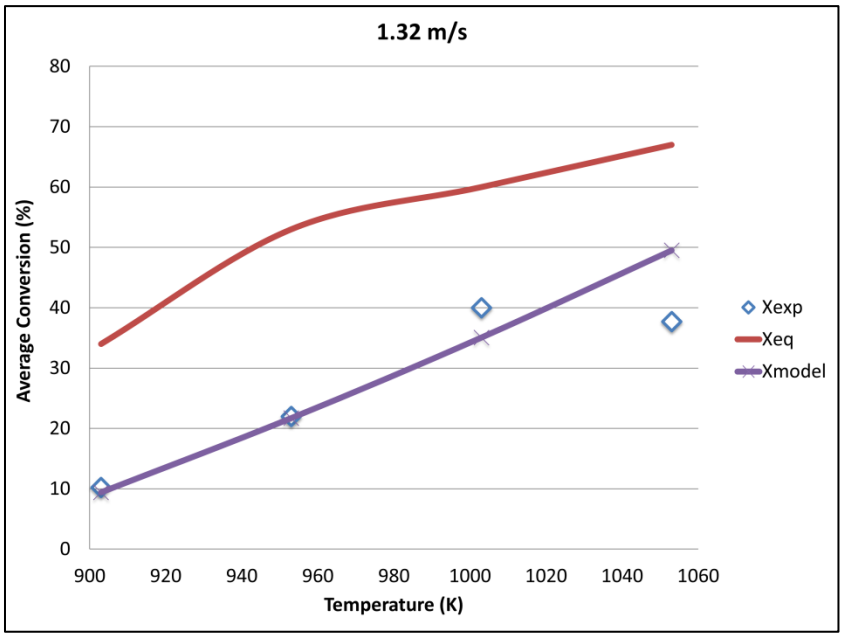

Figure 6-18: Average conversion by model versus experimental for flow: 1.32 m/s

The model prediction for average conversion achieved versus experimental data is overall very accurate for the various process conditions. Specifically the temperatures of 903, 953 and 1003 K the predictions are very accurate. An average error of 11% was obtained between experimental results and model prediction of the average outlet conversion for most of the experimental results. However, the error for inlet velocity 1.23 and 1.32 m/s at 1053 K are very large (53 and 31% respectively). The conversion achieved at higher temperatures deviates by quite an extent and it was difficult to assign an error to the

experimental data or the model. Although the conversion achieved was away from the overall equilibrium, a large enough distinction could not be made justifying the decision to use a reversible reaction rate. The other discrepancy in the model could be the fact that diffusion coefficients were calculated by correlations in literature and not evaluated experimentally. The effective diffusivity used inside the catalyst particles is highly dependent on the pore diameter in Knudsen diffusion and since all the particles were sintered together the particles at the highest temperature had longer exposure to the high temperature and thus could have reduced more in pore diameter size, resulting in inaccurate results. A more accurate representation of the particles could be achieved if characterization was to be done at all various process conditions.

(IV) Pressure Drop

A comparison of the pressure drop model predictions with experimental measurements were also attempted for the short catalyst beds (100mms) but the results were found to be different. This difference was attributed to the lack of reliability (placing) and sensitivity of the pressure transducers with measured differences of the order of 1 to 2 kPa. Other factors that could have attributed to this difference could include the physical properties of the catalyst particles (size and surface properties) which were difficult to account for in the model (DigiPac™) and which can have a significant influence on the porosity and consequently on the pressure drop. The geometry (packing) is very difficult to represent accurately, especially with irregular cylindrical shapes causing a large pellet size distribution.

More accurate numerical results could be obtained with regard to pressure drop if constant size pellets were to be used, so that the geometry could be based on that pellet size distribution. The detailed examination of the particle properties on pressure drop was not examined further in this investigation as a result of the uncertainty of measurement of very low pressure drops in a catalyst bed. Due to the inaccuracy of the void fraction, the effect of recirculation on the pressure drop could not be established. The predicted pressure drop was however compared with results derived from the Ergun equation (Ergun, 1952) given below with the model porosity (0.48). See Appendix A.

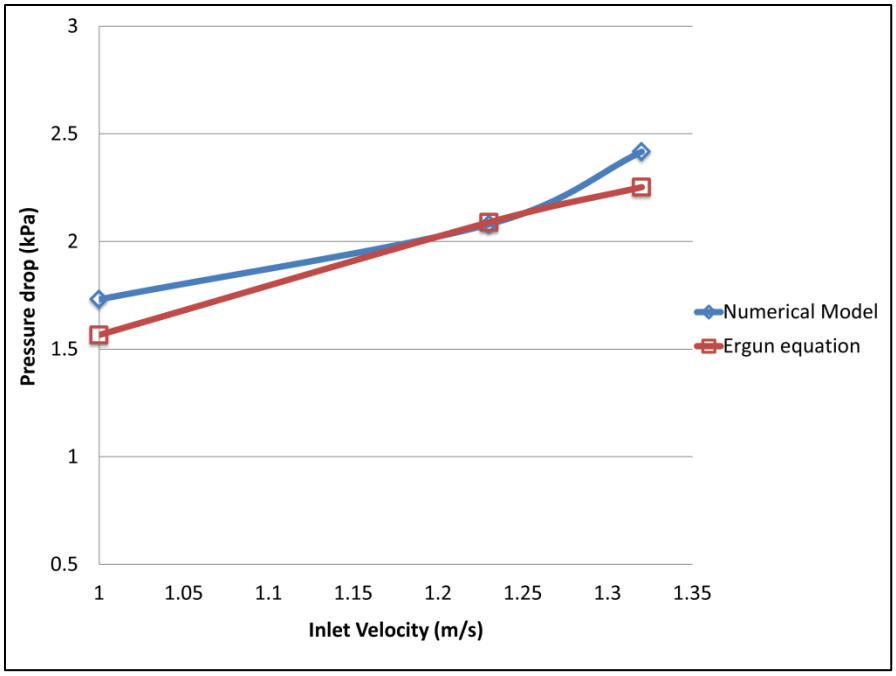

Figure 6-19: Pressure drop comparison between numerical model and Ergun equation

(V) Effect of Porosity on Heat Transfer

The effective radial thermal conductivity as a combination of convection and radiation in the fluid phase was incorporated by using the empirical correlation by Bauer and Schlünder (1978). A sensitivity analysis was done to investigate the effect of porosity in the heat transfer in the bed. The correlation from Bauer & Schlünder (1978) was varied as a function of emissivity, which included the following:

- Combined conduction, convection and radiation for porosity 0.36 and 0.48
- Combined convection and radiation for 0.36 and 0.48

The sensitivity analysis conducted with the empirical correlation from Bauer and Schlünder (1978) can be seen in Figure 6-20.

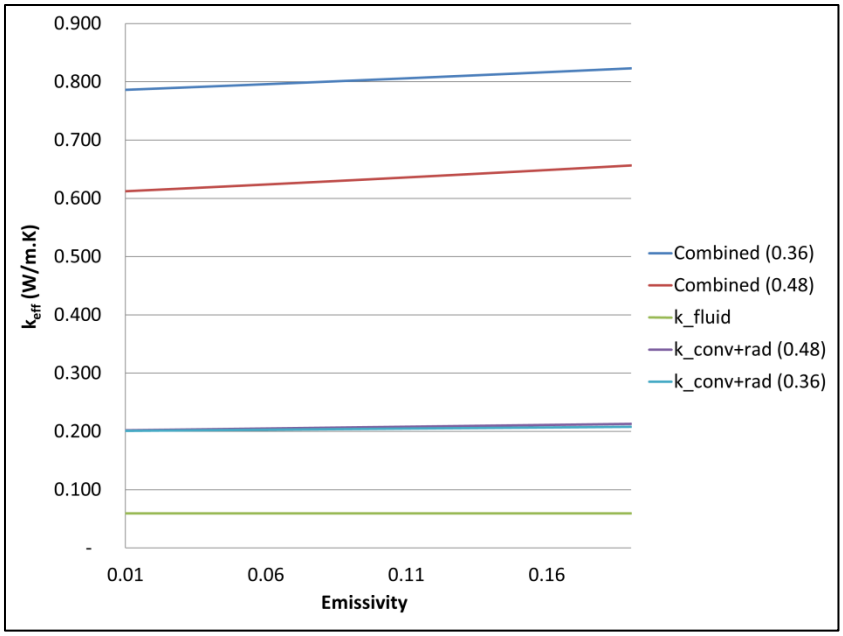

Figure 6-20: Effective radial thermal conductivity from empirical correlation

The effective thermal conductivity used in the model was 0.2 W/m.K which included convection and radiation in the fluid phase. Since the heterogeneous model incorporated conduction separately it was excluded from the adjusted value. From Figure 6-20 it can be seen that for combined conduction-convection-radiation combination the porosity had a large effect on the effective radial thermal conductivity and thus the heat transfer through the bed. For this instance where conduction was excluded from the effective fluid transfer coefficient (convection-radiation) a change in porosity did not alter the results. Since the bed generated by DigiPac™ had a porosity of 0.48 the total effective radial thermal conductivity would be different from the experimental thermal conductivity due to the lower porosity of 0.36.

6.6 Summary

The advance model delivered accurate results with regard to average conversion achieved by the model, compared with experimental results. For lower temperatures (903 K to 1003 K) the conversion predicted was accurate, whilst for the highest temperature of 1053 K (inlet) the predictions deviated from experimental results and the discrepancy could not be assigned to the model or faulty experiments. The centreline temperature comparison with probe measurements was never above a 2%

error and for most points it was below 1.5% for all for the experimental data, which was satisfactory. Radial temperature profiles were observed while radial concentration profiles seemed to be less observable. The influence of the reversible reaction rate could be observed where the reaction was inhibited as products started forming. For most of the average conversion model predictions the error was within 15% compared with experimental results with the exception of the highest operating temperature.

The numerical model was compared with the analytical solution by the Ergun pressure drop equation and the Ergun predicted pressure drop was close to that of the model. Radiation was successfully implemented by means of an empirical correlation and it was observed that the porosity did not have a large impact on convection and radiation (radial heat transfer) alone but on the combined effective radial thermal conductivity (solid conductivity included). Overall, the model provided accurate predictions with the advantage that the effects of heat mass transfer limitations are accounted for to truly get an accurate representation of the system under investigation.